Geomorphology 426 (2023) 108615

Contents lists available at ScienceDirect

Geomorphology

journal homepage: www.journals.elsevier.com/geomorphology

Geometry of last glacial sorted nets from high-resolution airborne data

Tomáš Uxa [a,*], Marek Křížek [b], Tereza Dlabáčková [b,c], David Krause [b,d]

[a] Institute of Geophysics, Czech Academy of Sciences, Boční II 1401, 141 31, Prague 4 – Spořilov, Czech Republic
[b] Department of Physical Geography and Geoecology, Faculty of Science, Charles University, Albertov 6, 128 43, Prague 2, Czech Republic
[c] Czech Geological Survey, Klárov 3, 118 21, Prague 1, Czech Republic
[d] The Krkonoše Mountains National Park Administration, Dobrovského 3, 543 01 Vrchlabí, Czech Republic

ARTICLE INFO

Keywords:
Patterned ground
Remote sensing
Permafrost
Palaeo-climate
Quaternary environments
Central Europe

ABSTRACT

Relict periglacial sorted nets are valuable indicators of past permafrost and climate states, but their field studies are usually challenging due to high time requirements and poor visibility. This study therefore tests the suitability of high-resolution digital elevation model and aerial photographs with a horizontal resolution of 0.5 m and 0.2 m, respectively, to map and analyse the geometry of 2000 sorted nets from the Last Glacial Period at one site in the Krkonoše Mts., Czech Republic. Since the sorted nets occupy an area of ~1.79 ha, the density of their network accounts for ~1117 cells per hectare. The sorted nets have a mean diameter of 3.46 ± 0.83 m, a mean height of 0.28 ± 0.10 m, and a mean estimated sorting depth of 0.94 ± 0.22 m. The number of sides ranges between three and ten, but averages 5.99 ± 1.13, and 83.4 % of the sorted nets are pentagonal to heptagonal, and their sides mostly meet at three-way junctions at a mean angle of 119.9 ± 25.6°. However, isometric sorted nets are rather rare as a length-to-width ratio attains 1.47 ± 0.28. The estimated sorting depth indicates that permafrost superimposed by ~1 m thick active layer occurred at the study site at the end of the Last Glacial Period. Generally, the remotely sensed parameters of the sorted nets are consistent with field data previously collected at the same study site and literature reports including those on past regional environmental conditions. This proves the utility of the high-resolution airborne data to map and analyse the geometry of large sets of sorted patterns, which would be difficult in conventional field surveys. Consequently, remote sensing could bring a wealth of new information on sorted patterned ground and its characteristics from past and present periglacial landscapes, and aid in past permafrost and climate modelling. The collected dataset of the parameters of the sorted nets could also have many other applications such as for choosing an effective sample size or the minimum network size to be included in statistical comparisons in future patterned-ground surveys, and for validating automated mapping and/or delineation tools and models of patterned-ground growth.

1. Introduction

Periglacial sorted nets are regular alternations of fine and coarse ground particles arranged in net-like patterns on the order of decimetres to meters in size, which are produced by recurrent freeze-thaw-induced processes that mainly operate under permafrost conditions (e.g., Ballantyne, 2013, 2018; Warburton, 2013; Harris et al., 2018). Since the patterned-ground development involves differential frost heave associated with mass displacements that may act on centennial to millennial timescales (Hallet, 2013; Kääb et al., 2014), it also greatly affects surface and subsurface water and energy fluxes, soil formation, vegetation composition, and/or biogeochemical cycling (Walker et al., 2008; Ping et al., 2015). Active sorted patterns mostly arise in level to moderately sloping terrains of polar, sub-polar, or alpine environments, but their relict counterparts also occur in many temperate regions outside the current periglacial realm where climate was colder in the past (Washburn, 1980; Ballantyne, 2013, 2018). Sorted patterned ground is therefore a valuable indicator of present and past permafrost and climate states (Goldthwait, 1976; Washburn, 1980; Grab, 2002; Ballantyne, 2013, 2018).

Sometimes, sorted patterns are isolated, but more commonly they occur in clusters that can have up to thousands of cells covering large areas if the topography and sediment supply are favourable. However, field explorations of such extensive assemblages are challenging due to high time requirements and poor visibility of relict sorted patterns at ground level. At most, tens to lower hundreds of cells have therefore

* Corresponding author at: Institute of Geophysics, Czech Academy of Sciences, Boční II 1401, 141 31, Prague 4 – Spořilov, Czech Republic.
E-mail address: uxa@ig.cas.cz (T. Uxa).

https://doi.org/10.1016/j.geomorph.2023.108615
Received 14 October 2022; Received in revised form 27 January 2023; Accepted 31 January 2023
Available online 2 February 2023

been surveyed at individual sites by most studies (e.g., Ballantyne and Matthews, 1982; Francou et al., 2001; Holness, 2003; Křížek and Uxa, 2013; Treml et al., 2010; Feuillet et al., 2012; Uxa et al., 2017). This results in rather limited datasets, especially for relict sorted patterned ground, which may not be fully representative and which usually consist only of general and easily measurable parameters that are readily visible from a ground perspective such as pattern length, width, or height.

Recent developments in the acquisition of high-resolution digital elevation models (DEMs) and aerial photographs using unmanned aerial vehicles, manned aircrafts, or satellites have made it possible to rapidly collect a wealth of information on various landforms, including periglacial ones, over extensive areas, which would be difficult by conventional field methods (e.g., Smith and Pain, 2009; Smith et al., 2016; Anderson et al., 2019). Notwithstanding that, remotely sensed data have so far been used at a relatively few sites only to examine the occurrence or dynamics of active to semi-active (Kääb et al., 2014; Dąbski et al., 2017; Berthling et al., 2020; Pereira et al., 2020) or relict (Evans et al., 2017; Křížek et al., 2019; Mather et al., 2019; Groos et al., 2021) sorted patterned ground. Detailed analyses of the geometry of large sets of sorted patterns are not yet available. Most work on the geometry of patterned ground has been made for active (Haltigin et al., 2012; Lousada et al., 2018; Bernard-Grand'Maison and Pollard, 2018; Zhang et al., 2018, 2020; Abolt et al., 2019; Bhuiyan et al., 2020; Witharana et al., 2020, 2021; Rettelbach et al., 2021; Chiasson and Allard, 2022) and relict (Andrieux et al., 2016; Ewertowski et al., 2017; Beerten et al., 2021; Bertran, 2022) thermal-contraction-cracking polygons, which are typically tens of meters in diameter and therefore easier to detect compared to generally much smaller sorted patterns.

This study therefore tests the suitability of a region-wide high-resolution DEM and aerial photographs for the manual detection and delineation of a large number of sorted nets from the Last Glacial Period (~115–11.7 ka) at one site in the Krkonoše Mts., Czech Republic, and for determining their surface geometry and estimating their subsurface extent (~sorting depth). Consequently, it analyses the collected geometric parameters of the sorted nets and their relationships, and evaluates them using field data and literature reports including those on past regional environmental conditions.

2. Study area

The Krkonoše Mts. are ~40 km long WNW-ESE oriented Variscan fault-block mountain range (Chlupáč et al., 2011) on the Czech–Polish border (Fig. 1) that is composed of crystalline rocks (Chaloupský et al., 1989). The range is characterized by extensive forest-free summit surfaces of low relief at ~1300–1450 m asl, with mostly gentle hills and saddles rising up to ~100–150 m above, which are dissected by deep valleys (Migoń, 1999). The mountains have repeatedly faced much colder climate conditions during the Quaternary glaciations, which have left a distinct periglacial imprint on summit plateaus (Traczyk and Migoń, 2000; Křížek, 2007; Křížek et al., 2010, 2019), whereas several valleys exhibit glacier remodelling (Křížek et al., 2012; Engel et al., 2014; Krause et al., 2022). Most periglacial features such as cryoplanation terraces, tors, blockfields, stone-banked lobes, sorted polygons, nets, and stripes are believed to have developed and/or been last active towards the end of the Last Glacial Period (Traczyk and Migoń, 2000; Traczyk, 2004; Křížek et al., 2010; Engel et al., 2021) in the presence of permafrost (Czudek, 2005), but some seasonal-frost features such as small-scale sorted circles, peat hummocks, ploughing blocks, or small solifluction lobes are thought to have been active throughout the Holocene (Sekyra and Sekyra, 1995; Křížek et al., 2010; Křížek and Uxa, 2013).

The study was undertaken on the Luční pláň plateau (15°41′8″E, 50°43′34″N, 1530 m asl; Fig. 1) where there is an extensive network of relict sorted nets (Křížek, 2007; Křížek et al., 2019). The site is underlain by Neoproterozoic muscovite-chlorite schists and phyllites (Chaloupský et al., 1989) that are covered with a sand-gravel regolith of low to medium frost susceptibility (Sekyra and Sekyra, 1995). The sorted nets (Fig. 2) are superimposed by podzolic soils with a continuous grass cover (Kociánová and Sekyra, 1995), which indicate their long-term inactivity. However, well-preserved elevated centres surrounded by distinct troughs (Fig. 2) suggest that the sorted nets have been continuously forest-free, as tree-root activity would have otherwise flattened them (Sekyra et al., 2002; Treml et al., 2008). Cosmogenic ^{10}Be exposure dating of sorted polygons in the Krkonoše Mts. and nearby Hrubý Jeseník Mts. indicated that those patterns developed at ~30–18 ka (~most of the Marine Isotope Stage 2) with peak activity at ~25 ka (~Last Glacial Maximum) (Engel et al., 2021), and we assume that the sorted nets examined in this study had an analogous formation history. The mean annual air temperature at the highest peak of the Krkonoše Mts., Mt. Sněžka (1603 m asl), located ~4 km east of the study site, was 0.4 °C in 1961–1990 (Coufal et al., 1992) and 1.2 °C in 1981–2010 (Migała et al., 2016), and the mean annual precipitation was 1186 mm in 1961–2017 (Pińskwar et al., 2019). Snow cover at the study site usually lasts from November–December to April–May and can reach a maximum thickness of up to ~1.5–2 m (personal observations from 2009 to 2021). Ground temperatures are poorly known, and the only published and discontinuous series from two locations <1 km from the study site suggest that the mean annual ground temperature at a depth

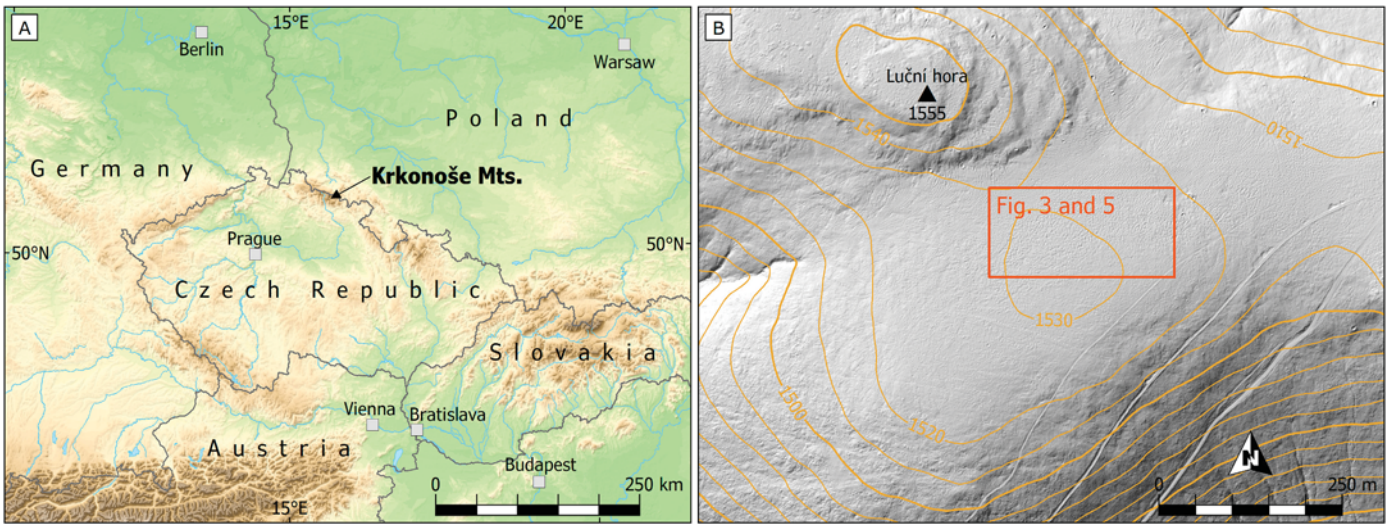

Fig. 1. (A) Location of the Krkonoše Mts. in Central Europe and (B) topography around the study site visualized using hillshade relief.

Fig. 2. (A) Overview of the sorted nets at the study site and (B) their close-up view captured during a geophysical survey. Note the dense grass cover on the sorted nets that hinders their recognition from a ground perspective despite the distinctive microtopography.

of 0.1 m was around 4 °C in 1999–2001 (Harčarik, 2002).

3. Data and methods

3.1. Remotely sensed data and mapping strategy

The sorted nets were examined using a LiDAR (light detection and ranging) DEM of the Krkonoše Mts. National Park (~550 km^2) with a horizontal resolution of 0.5 m derived from a point cloud with a mean density of 5 points per square meter acquired by airborne laser scanning (Puchrik and Nýdrle, 2013), which has an estimated vertical accuracy of better than 0.18 m. Additionally, true-colour orthogonal aerial photographs of the Czech Republic with a horizontal resolution of 0.2 m from the Czech Office for Surveying, Mapping, and Cadastre as well as two sets of aerial photographs accessible from Google Earth™ were utilized. The DEM subset for the study site was further used to derive rasters of topographic position index (calculated for each grid cell as its elevation minus the mean elevation within a radius of 2 m), slope inclination, and hillshade relief (with default azimuth and altitude angle of the light source of 315° and 45°, respectively) using ArcGIS 10.8 software (Esri Inc., 2019), which were normalized to values between 0 and 1 as follows:

$$x' = \frac{x - min(x)}{max(x) - min(x)}, \quad (1)$$

where x' is the normalized value of a grid cell, x is the original value of a grid cell, and min(x) and max(x) is the minimum and maximum raster value, respectively. The normalized rasters of inverse topographic position index and slope inclination were then subtracted from each other to obtain two additional combined rasters in which the sorted nets were more visible. Lastly, the rasters were refined by a cubic convolution resampling for display in ArcGIS 10.8 (Fig. 3).

The sorted nets were visually identified through colour contrasts between their centres and troughs discernible on the DEM-derived rasters and the aerial photographs (Fig. 3). The mapping targeted a flat to slightly inclined domain of ~1.79 ha where the sorted nets are most distinct and where there are no strongly elongated patterns affected by slope processes, which become dominant on slopes over ~4° in the Krkonoše Mts. (Křížek et al., 2019). There, a total of 2000 sorted nets were manually digitized by one operator so that their outlines were mostly drawn as single straight lines between pairs of polygon vertices that ran through the centres of the troughs (Fig. 4), and these were subsequently double-checked by another operator and amended by consensus if necessary. Local deflections were not considered when drawing the sides because they are small and the sides are short (~several meters) so we believe that no information is lost while increasing simplicity. Likewise, trough width was not considered because it is at the order of the DEM resolution whose derivatives were used as the primary basis for the identification and delineation of the sorted nets. Also, the troughs mostly have V-shaped transverse profiles, which means that their centres can be found easily, but the exact position of their limits is mostly unclear.

3.2. Remotely sensed parameters of the sorted nets

Geometry of the delineated sorted nets (Fig. 5) was examined using various tools available in ArcGIS 10.8. The horizontal geometry of each sorted net was characterized by a length (~maximum horizontal cell dimension), its azimuth, and a width (~largest cell extent perpendicular to the length) using the *RECTANGLE_BY_WIDTH* option of the *Minimum Bounding Geometry* tool. Subsequently, a pattern diameter was calculated as an arithmetic mean of the length and width to describe a typical horizontal dimension of each sorted net by a single value. A length-to-width ratio was established to evaluate the pattern symmetry. Sorted-net perimeter and area were determined using the *Calculate Geometry* tool. Single polygonal objects representing the individual sorted nets were then converted to polyline objects using the *Polygon To Line* tool and these were further divided into single mostly straight lines using the *Split Line At Vertices* tool. The number of these lines within each sorted net was assumed to be the number of its sides. Since the sorted nets were digitized by drawing single mostly straight lines between pairs of polygon vertices, we believe that the number of sides is in almost all instances equal to the number of neighbours. Side lengths and azimuths were determined using *Add Geometry Attributes* tool, which also allowed calculation of inner angles of the sides. Start vertices of the sides were then converted to points using the *Feature Vertices To Points* tool and the number of overlapping points was assumed to define the number of sides that meet at each vertex (except for points on the outer perimeter of the entire network of the sorted nets). The vertical geometry of each sorted net was described by its height, and mean and maximum slope of its surface, which characterize the elevation difference between the centre and troughs and the steepness of the slopes in between, respectively, and these were determined using the *Zonal Statistics as Table* tool on the basis of the DEM and DEM-derived slope inclination. Lastly, a sorting depth was estimated for each sorted net based on seventy-five published diameter—sorting depth pairs for active sorted patterned ground, which

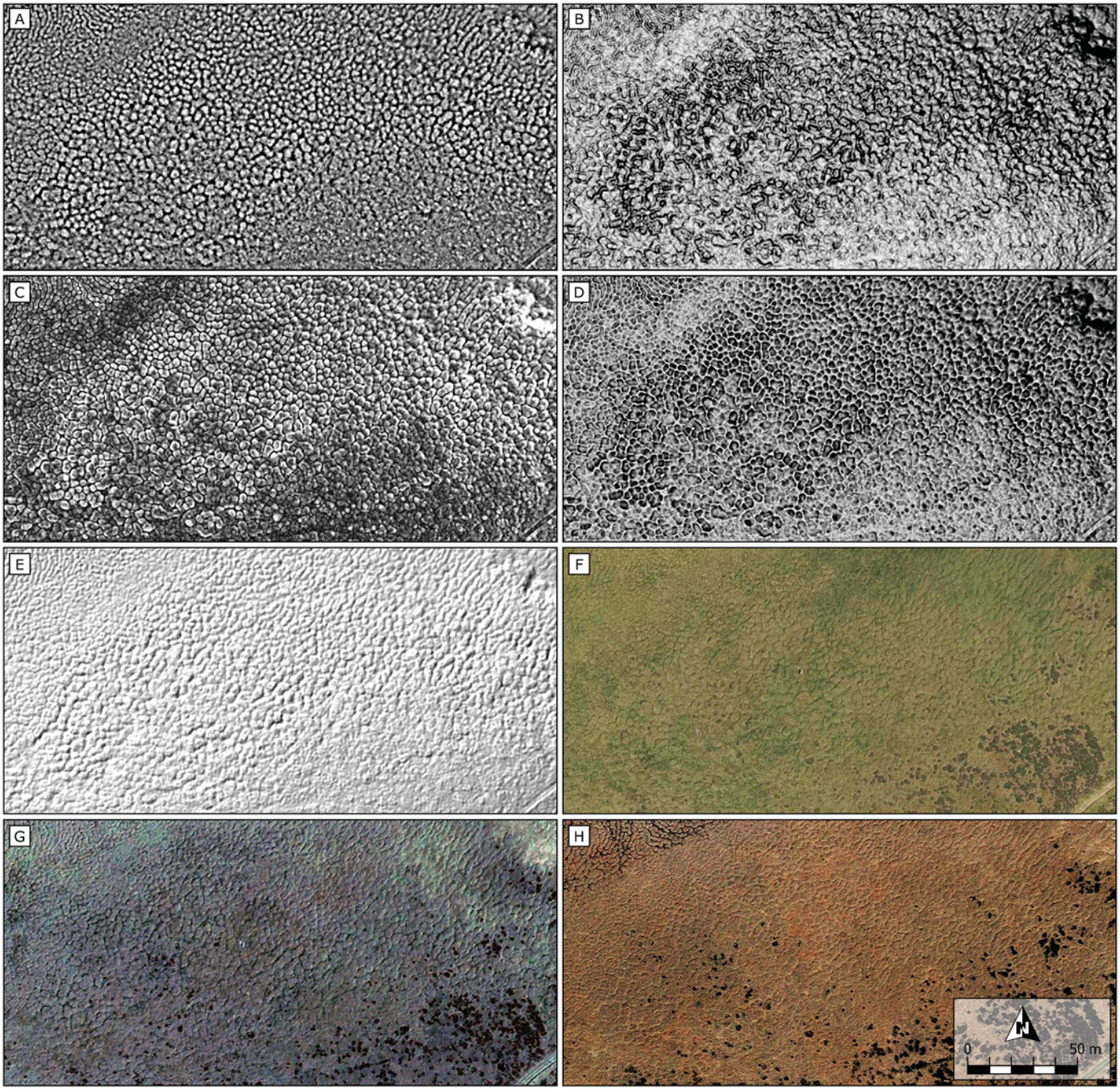

Fig. 3. Normalized DEM-derived rasters of (A) topographic position index, (B) slope inclination, (C) slope minus inverse topographic position index, (D) inverse topographic position index minus slope, (E) hillshade relief, (F) orthogonal aerial photograph from the Czech Office for Surveying, Mapping, and Cadastre, and (G, H) Google Earth™ images used to detect and delineate the sorted nets. Note that the orientation and scale shown in (H) is the same for all panels.

have the Pearson correlation coefficient of 0.97 and yield the following relationship (Fig. 6):

$$z = 0.2645d + 0.02, \quad (2)$$

where z [m] is the sorting depth and d [m] is the pattern diameter.

3.3. Field-based parameters of the sorted nets

Basic remotely sensed parameters of the sorted nets such as the length, width, diameter, and height were validated using field-based data previously collected for ninety-two sorted nets at the same study site (Křížek et al., 2007, 2010, 2019; Treml et al., 2010). The sorting depth was evaluated against published values from the study site (Sekyra and Sekyra, 1995) and other locations in the Krkonoše Mts. (Kunský and Záruba, 1950; Sekyra, 1960; Králík and Sekyra, 1969; Jahn, 1977; Sekyra et al., 2002) and also by an electrical resistivity tomography (ERT) sounding performed at the study site. The ERT survey was done on a 33.3 m long electrode array consisting of 112 nails with a spacing of 0.3 m, which crossed eight complete sorted nets (Fig. 5). The resistivity was measured using ARES II automatic resistivity system (GF Instruments Ltd.) in the Wenner–Schlumberger and dipole–dipole electrode configurations, which reached a maximum depth of ~6 m. The raw data were then processed using the robust inversion scheme in RES2DINV software (Geotomo Software) to produce a concatenated

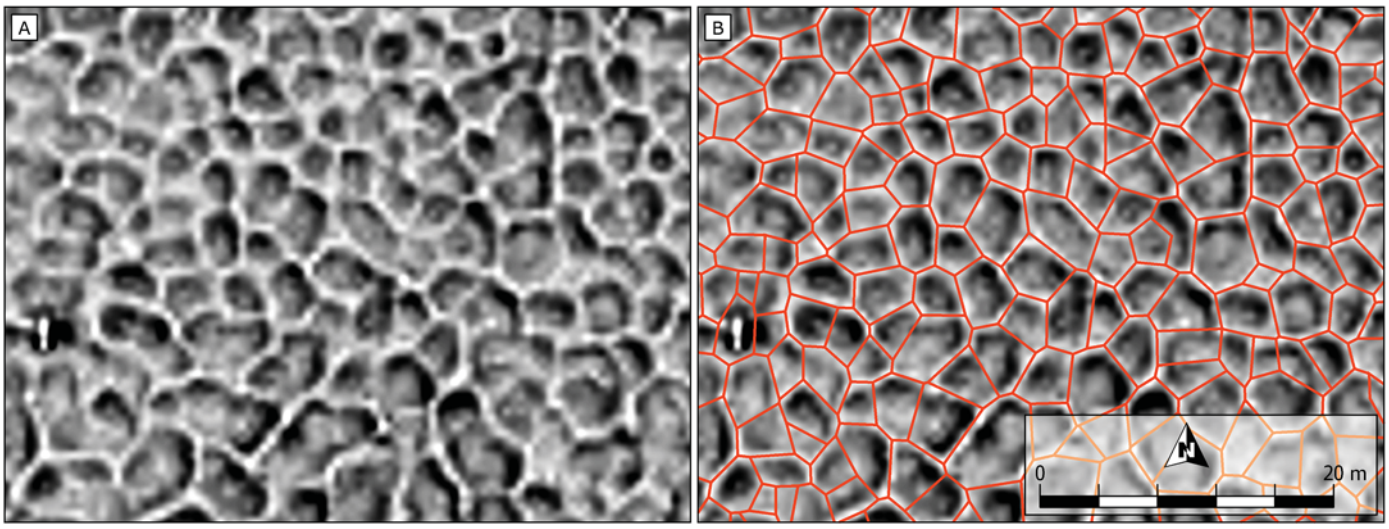

Fig. 4. Sample delineation of the sorted nets (orange polygons) in a subset of the study site based on the background raster of inverse topographic position index minus slope inclination. Note that the orientation and scale shown in (B) is the same for both panels.

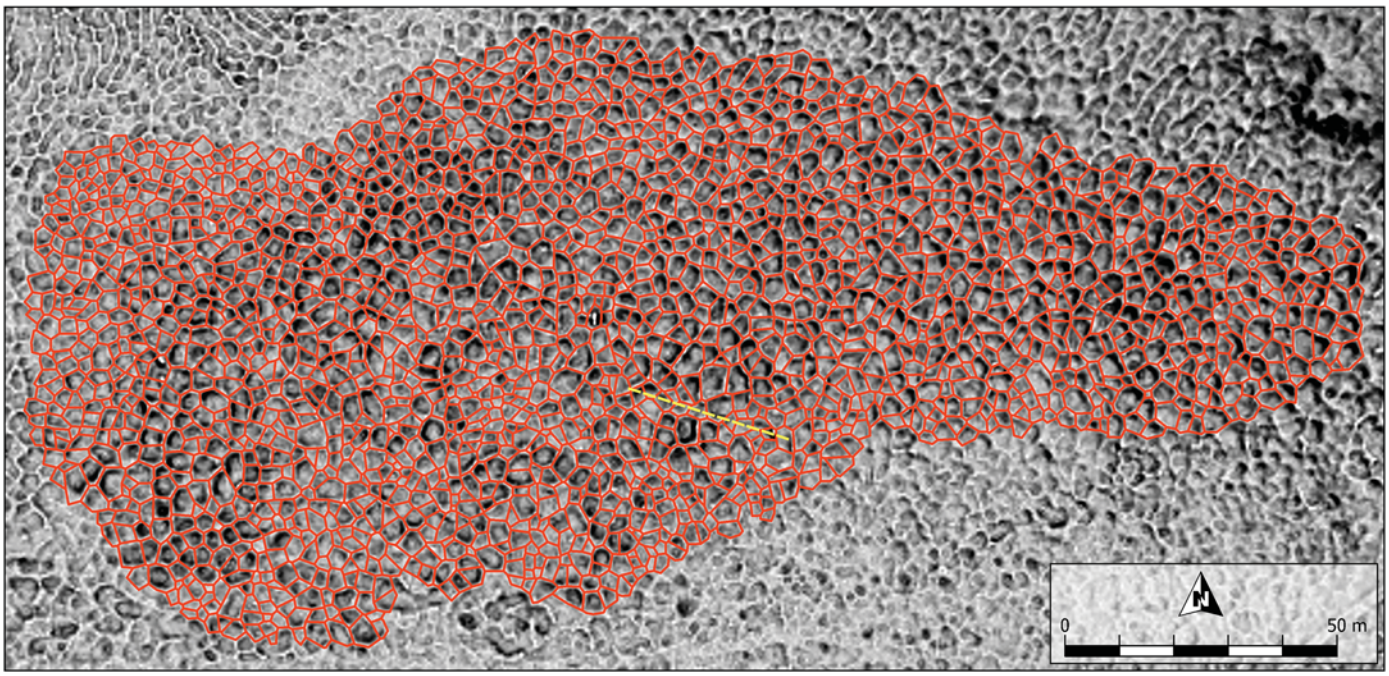

Fig. 5. Delineated network of the sorted nets (orange polygons) with the background raster of inverse topographic position index minus slope inclination. The yellow dashed line delineates the electrical resistivity profile used to validate the estimated sorting depth of the sorted nets (see Sect. 3.3).

resistivity tomogram, which combines both electrode configurations into a single output that better details the subsurface structures with sharp boundaries, which occur at the study site.

3.4. Data analysis

The parameters of the sorted nets were characterized with simple descriptive statistics such as an arithmetic mean, standard deviation, coefficient of variation, median, minimum, maximum, and quantiles. The length axes azimuths were classified into eighteen ten-degree wide bidirectional sectors so that, for instance, the eastern azimuths (85–95°) were considered equivalent to the western ones (265–275°). Probability distributions of the parameters of the sorted nets were assessed using probability density plots and their adherence to individual distributions was tested by means of log-likelihood, and Akaike and Bayesian information criterions using the *fitdistrplus* R package (Delignette-Muller and Dutang, 2015). Relationships between the parameters of the sorted nets were evaluated using the Pearson correlation coefficient tested at $p < 0.001$. Lastly, the number of observations required for the mean values of the parameters of the sorted nets to be constantly below certain absolute percentage errors (0.1 to 20 %) were searched by repeatedly choosing the individual parameter observations in random order and then computing their cumulative means. A hundred thousand random combinations were simulated for each parameter to achieve stable outputs for descriptive statistics and to determine the minimum data dimension to yield significant results on the given network of sorted nets.

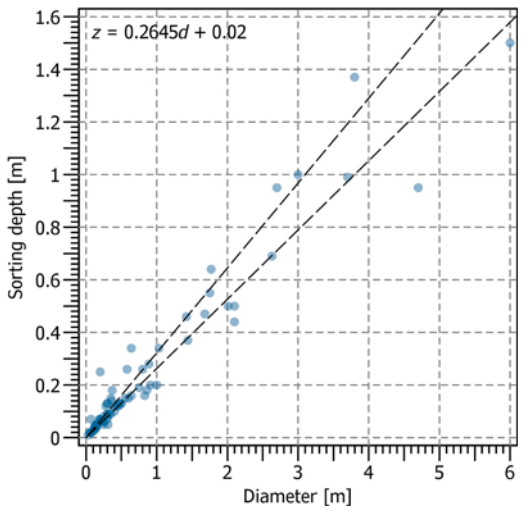

Fig. 6. Relationship between the diameter (d) and sorting depth (z) based on seventy-five previously published values for active sorted patterned ground (Troll, 1944; Furrer, 1955; Sekyra, 1969; Bunting and Jackson, 1970; Freund, 1971; Graf, 1973; Ellenberg, 1976; Ballantyne and Matthews, 1982; Ray et al., 1983; Gleason et al., 1986; Hallet and Prestrud, 1986; Walters, 1988; Cook, 1989; Van Vliet-Lanoë, 1991; Wilson and Clark, 1991; Wilson, 1992; Ballantyne and Harris, 1994; Kück, 1996; Grab, 1997; Kling, 1997; Humlum and Christiansen, 1998; Holness, 2003; Dąbski, 2005; Uxa et al., 2017), which was used to estimate the sorting depth of the sorted nets at the study site. The diagonal black dashed lines indicate the theoretical range of the diameter-to-sorting depth ratio of ~3.1–3.8 (Ray et al., 1983; Gleason et al., 1986; Hallet and Prestrud, 1986; Krantz, 1990).

4. Results

4.1. Descriptive statistics of the remotely sensed parameters of the sorted nets

The remotely sensed sorted nets have a mean length and width of 4.08 ± 1.02 m and 2.83 ± 0.75 m, respectively, which yields a mean diameter of 3.46 ± 0.83 m, and their mean side length reaches 1.93 ± 0.92 m (Table 1). The smallest cell has a diameter of 0.97 m, while the largest one attains 6.13 m; 90 % of the total sample are, however, between 2.12 m and 4.94 m. The centres of the sorted nets stand at a mean height of 0.28 ± 0.10 m above the bordering troughs, but range between flat ones, which are as low as 0.04 m, and elevated ones, which rise up to 0.86 m (Table 1). The surfaces of the sorted nets have a mean slope of 5.5 ± 1.4° and a mean maximum slope of 11.4 ± 3.4°; the highest maximum slope is 26.2° (Table 1). The mean sorting depth estimated from the remotely sensed diameter of the sorted nets using the Eq. (2) is 0.94 ± 0.22 m. It oscillates between 0.28 m and 1.64 m, but 90 % of the total sample are between 0.58 m and 1.33 m (Table 1). Since the 2000 sorted nets occupy a total area of ~1.79 ha, the density of their network accounts for ~1117 cells per hectare, and their mean area is 8.95 ± 4.28 m^2. Whereas the smallest sorted net has an area of <1 m^2, the largest one achieves 28.5 m^2. The mean cell perimeter equals 11.55 ± 2.65 m (Table 1).

The number of sides of the sorted nets ranges between three and ten, but averages 5.99 ± 1.13 (Table 1), and 98.2 % of them have four to eight sides. Most of the sorted nets are hexagonal, 34.5 % of the total sample; pentagonal and heptagonal sorted nets also occur abundantly, representing 26.6 % and 22.3 %, respectively, while tetragonal and octagonal ones account for 7.9 % and 6.9 % of the total sample, respectively (Fig. 7). The sides predominantly meet at three-way junctions at a mean angle of 119.9 ± 25.6° (Table 1). Despite that, isometric cells are rather rare, as a length-to-width ratio of the sorted nets attains 1.47 ± 0.28 (Table 1) and 4.6 % of them exhibit values larger than 2. However, the length axes of the sorted nets have no preferred orientation and are rather evenly distributed across all the eighteen bidirectional sectors (Fig. 8), which account for 4.2–7.2 % of the total sample.

4.2. Probability distributions of the remotely sensed parameters of the sorted nets

Most of the parameters of the sorted nets (Table 1) are best

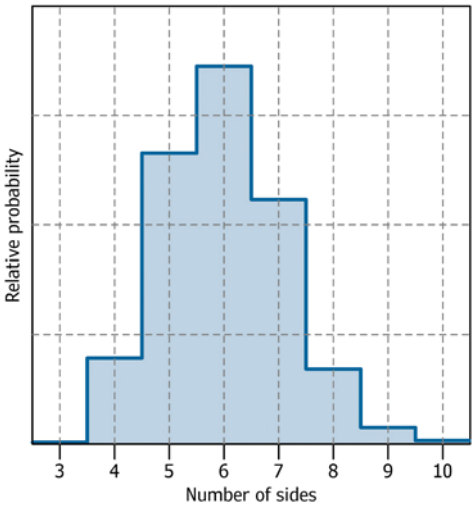

Fig. 7. Frequency distribution of the remotely sensed number of sides of the sorted nets.

Table 1
Descriptive statistics of the remotely sensed parameters of the sorted nets (n = 2000).

Parameter	μ	σ	c_v	P_{50}	Min	Max	P_5	P_{10}	P_{25}	P_{75}	P_{90}	P_{95}
Length [m]	4.08	1.02	0.25	4.03	0.98	7.79	2.48	2.78	3.39	4.75	5.40	5.82
Width [m]	2.83	0.75	0.26	2.79	0.90	5.18	1.66	1.89	2.31	3.34	3.83	4.16
Length-to-width [–]	1.47	0.28	0.19	1.42	1.01	2.92	1.11	1.16	1.26	1.62	1.84	1.98
Diameter [m]	3.46	0.83	0.24	3.43	0.97	6.13	2.12	2.40	2.87	4.01	4.56	4.94
Height [m]	0.28	0.10	0.37	0.27	0.04	0.86	0.13	0.15	0.21	0.35	0.42	0.46
Sorting depth [m]	0.94	0.22	0.24	0.93	0.28	1.64	0.58	0.65	0.78	1.08	1.23	1.33
Number of sides	5.99	1.13	0.19	6.00	3.00	10.00	4.00	5.00	5.00	7.00	7.00	8.00
Side length [m]	1.93	0.92	0.48	1.88	0.07	5.63	0.48	0.72	1.27	2.56	3.17	3.54
Side inner angle [°]	119.9	25.6	0.21	120.1	39.3	180.0	77.0	86.2	102.1	137.9	153.6	162.4
Perimeter [m]	11.55	2.65	0.23	11.52	3.59	20.7	7.20	8.17	9.72	13.28	14.92	16.09
Area [m^2]	8.95	4.28	0.48	8.32	0.80	28.5	3.13	3.99	5.77	11.41	14.65	17.09
Mean slope [°]	5.5	1.4	0.25	5.5	1.6	10.6	3.2	3.7	4.5	6.4	7.2	7.7
Maximum slope [°]	11.4	3.4	0.30	11.3	2.5	26.2	6	7	8.9	13.7	15.9	17.2

μ = arithmetic mean; σ = standard deviation; c_v = coefficient of variation; P_{50} = median; Min = minimum value; Max = maximum value; P_5, P_{10}, P_{25}, P_{75}, P_{90}, and P_{95} = 5th, 10th, 25th, 75th, 90th, and 95th percentile, respectively.

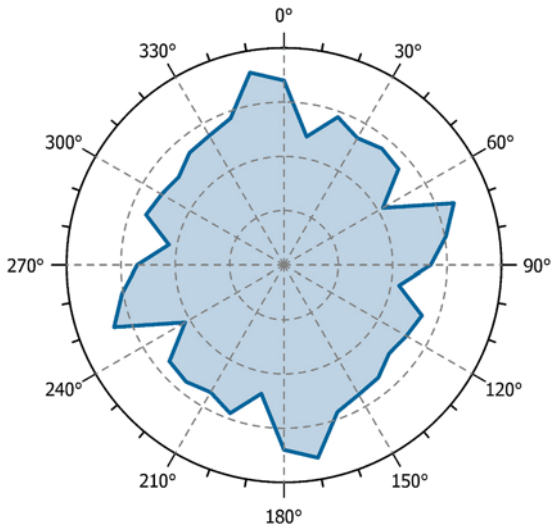

Fig. 8. Frequency distribution of the remotely sensed azimuths of the length axes of the sorted nets.

characterized by normal distribution (diameter, sorting depth, perimeter, side length, side inner angle, and mean and maximum slope of the surface of the sorted nets) that may show a subtle skew to the right (Fig. 9). Other parameters are somewhat more skewed and best fit gamma (length, width, height, number of sides, and area) or lognormal (length-to-width ratio) distributions (Fig. 9). The only exception is the length axis azimuth, which is distributed uniformly (Fig. 8).

4.3. *Relationships between the remotely sensed parameters of the sorted nets*

The parameters of the sorted nets are mostly significantly moderately to highly correlated (Table 2). The highest correlation coefficients mostly above ~0.90 exhibit such parameters as the length, width, diameter, sorting depth, perimeter, and area (Table 2; Fig. 10). Correlation coefficients of the other parameters mostly achieve ~0.30–0.70. The only exception is the length-to-width ratio, which largely shows much weaker and statistically non-significant correlations with the other parameters of the sorted nets (Table 2), and we suspect this is because the study site is generally flat and the length axes azimuths of the sorted nets therefore have no preferential orientation, which causes the length-to-width ratio to be more or less randomly related to most of the other parameters. Most of the parameter associations are positive linear (Table 2), but positive power function most closely fits the

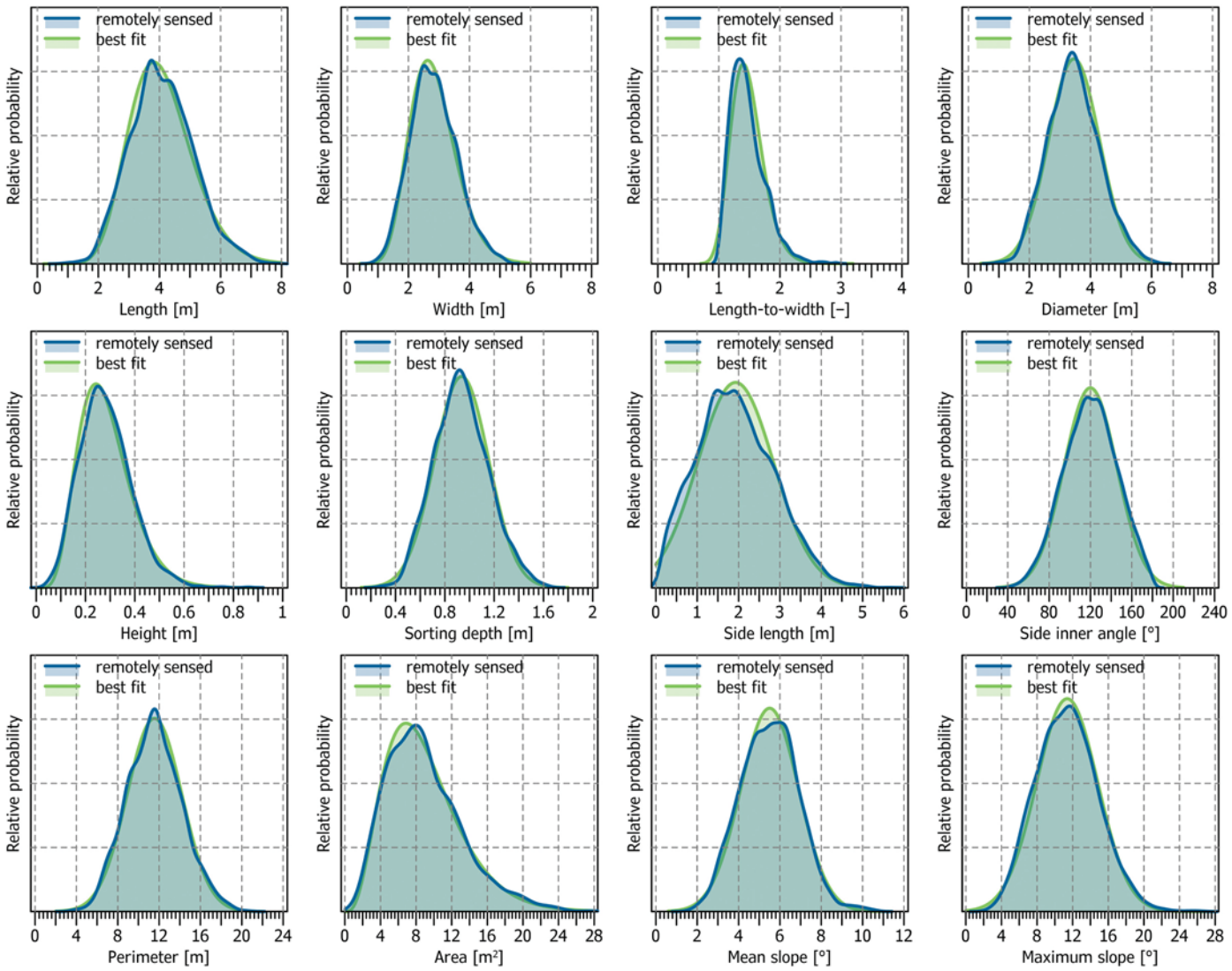

Fig. 9. Probability density of the remotely sensed parameters of the sorted nets along with their best-fit distribution functions.

Table 2
Pearson correlation coefficients between the remotely sensed parameters of the sorted nets. Statistically significant correlations ($p < 0.001$) are shown in bold.

Parameter	Length	Width	Length-to-width	Diameter	Height	Sorting depth	Number of sides	Mean side length	Mean side inner angle	Perimeter	Area	Mean slope	Maximum slope
Length		**0.76**	**0.26**	**0.96**	**0.64**	**0.96**	**0.61**	**0.55**	**0.60**	**0.94**	**0.89**	**0.35**	**0.52**
Width	**0.76**		**−0.40**	**0.92**	**0.64**	**0.92**	**0.62**	**0.49**	**0.61**	**0.91**	**0.93**	**0.41**	**0.55**
Length-to-width	**0.26**	**−0.40**	–	−0.02	−0.07	−0.02	−0.07	0.05	**−0.08**	−0.03	**−0.12**	**−0.12**	**−0.10**
Diameter	**0.96**	**0.92**	−0.02	–	**0.68**	**1.00**	**0.66**	**0.56**	**0.64**	**0.99**	**0.97**	**0.40**	**0.57**
Height	**0.64**	**0.64**	−0.07	**0.68**	–	**0.68**	**0.40**	**0.46**	**0.40**	**0.70**	**0.67**	**0.79**	**0.84**
Sorting depth	**0.96**	**0.92**	−0.02	**1.00**	**0.68**	–	**0.66**	**0.56**	**0.64**	**0.99**	**0.97**	**0.40**	**0.57**
Number of sides	**0.61**	**0.62**	−0.07	**0.66**	**0.40**	**0.66**	–	**−0.22**	**0.97**	**0.64**	**0.67**	**0.20**	**0.32**
Mean side length	**0.55**	**0.49**	0.05	**0.56**	**0.46**	**0.56**	**−0.22**	–	**−0.22**	**0.59**	**0.51**	**0.32**	**0.41**
Mean side inner angle	**0.60**	**0.61**	**−0.08**	**0.64**	**0.40**	**0.64**	**0.97**	**−0.22**	–	**0.63**	**0.64**	**0.20**	**0.32**
Perimeter	**0.94**	**0.91**	−0.03	**0.99**	**0.70**	**0.99**	**0.64**	**0.59**	**0.63**	–	**0.97**	**0.42**	**0.58**
Area	**0.89**	**0.93**	**−0.12**	**0.97**	**0.67**	**0.97**	**0.67**	**0.51**	**0.64**	**0.97**	–	**0.39**	**0.56**
Mean slope	**0.35**	**0.41**	**−0.12**	**0.40**	**0.79**	**0.40**	**0.20**	**0.32**	**0.20**	**0.42**	**0.39**	–	**0.84**
Maximum slope	**0.52**	**0.55**	**−0.10**	**0.57**	**0.84**	**0.57**	**0.32**	**0.41**	**0.32**	**0.58**	**0.56**	**0.84**	–

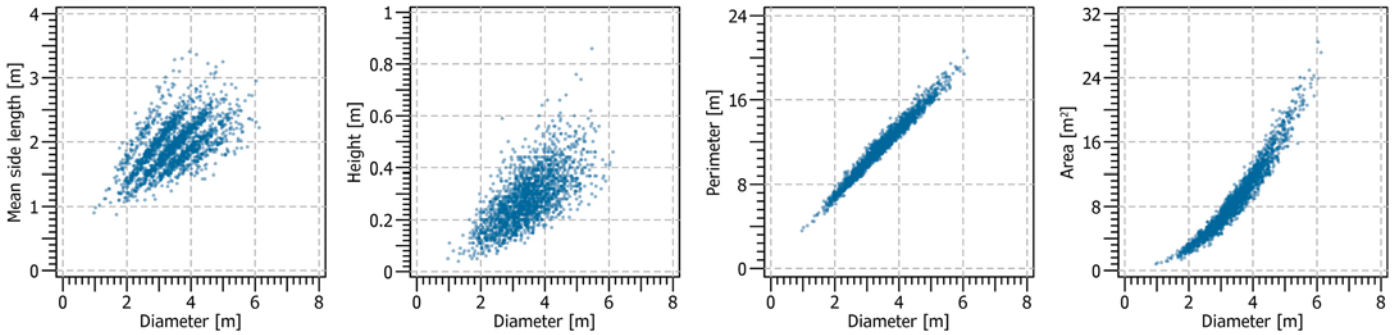

Fig. 10. Sample relationships between the remotely sensed diameter of the sorted nets and selected other parameters.

relationship of the cell area to most of the other parameters (Fig. 10). Likewise, the number of sides positively linearly relates to most of the other parameters; however, the mean side length tends to shorten as the number of sides rises (Table 2, Fig. 11).

4.4. Relationships between the remotely sensed parameters of the sorted nets and their number of observations

The absolute percentage error of the mean values of the remotely sensed parameters of the sorted nets decrease exponentially with the number of their observations (Fig. 12). Most of the parameters typically require less than ~30 and ~30–100 observations for the absolute percentage error to be constantly below 10 % and 5 % of the mean parameter value, respectively (Table 3). However, there are substantial differences in the number of observations required among the individual parameters of the sorted nets, and these increase as the errors decrease (Fig. 12). The typical number of observations required for the absolute percentage error to be constantly below 2 % therefore varies between ~100 and ~550, while for the error to be constantly below 1 % it mostly spans as much as between ~350 and ~1200 (Table 3). The lowest number of observations is needed for the length-to-width ratio and number of sides, while the highest number of observations is required for the height, side length, and area (Table 3).

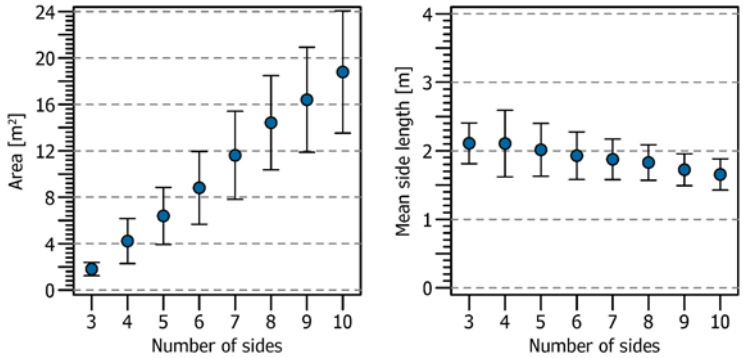

Fig. 11. Sample relationships between the remotely sensed number of sides of the sorted nets and selected other parameters.

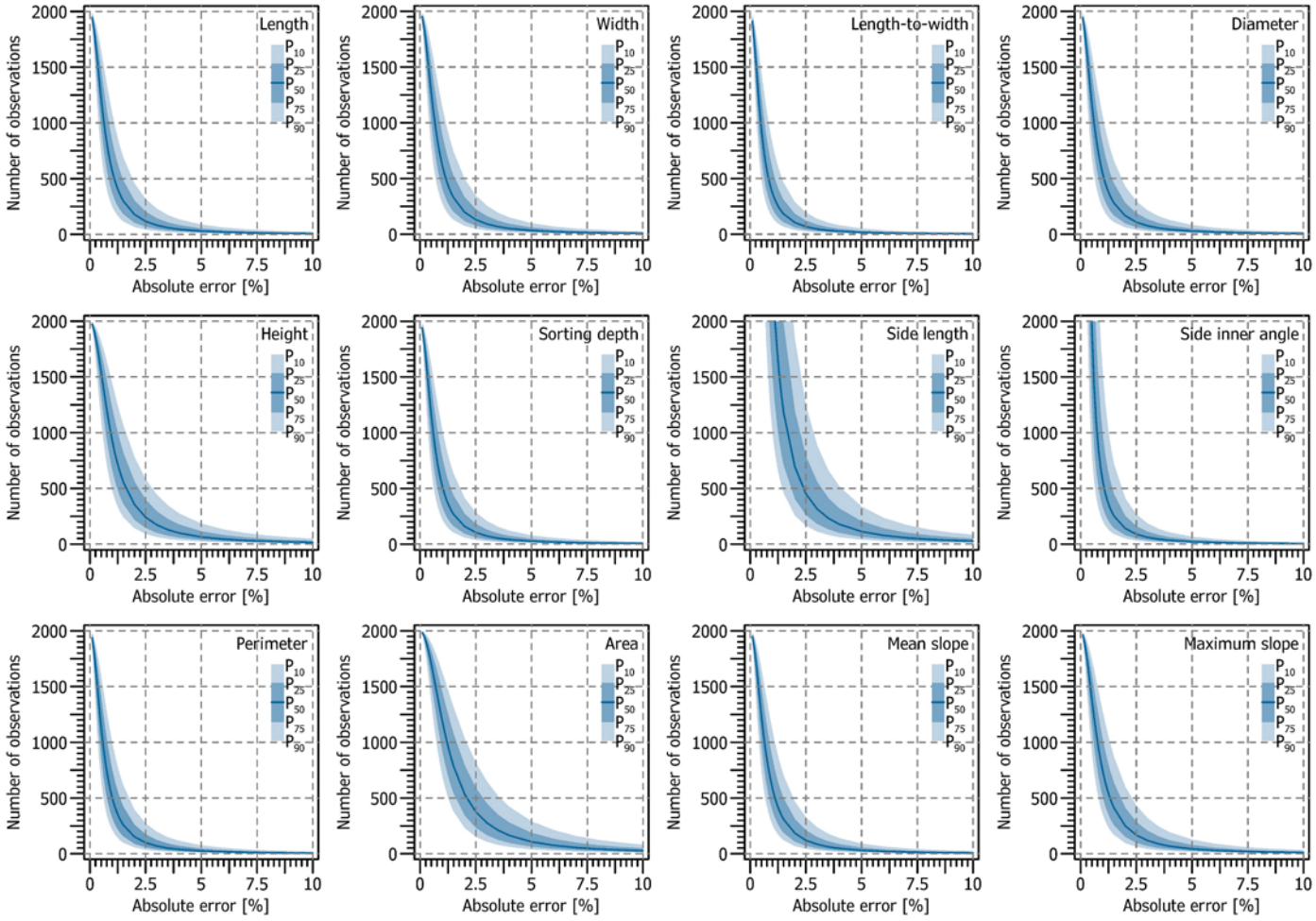

Fig. 12. Number of observations needed for the mean values of the remotely sensed parameters of the sorted nets to be constantly below the given absolute percentage errors. The percentiles are reported due to highly skewed distributions.

Table 3
Median number of observations needed for the mean values of the remotely sensed parameters of the sorted nets to be constantly below the given absolute percentage errors. The medians are reported due to highly skewed distributions.

Parameter	20 %	15 %	10 %	5 %	4 %	3 %	2 %	1 %
Length	2	3	7	29	46	82	178	570
Width	2	3	8	33	52	91	198	619
Length-to-width	1	2	4	16	26	47	106	372
Diameter	2	3	6	27	43	76	166	537
Height	4	7	15	64	100	173	354	927
Sorting depth	2	3	6	26	41	72	160	523
Number of sides	1	2	4	17	26	47	103	367
Side length	6	12	27	113	177	314	695	2386
Side inner angle	1	2	5	21	34	61	141	554
Perimeter	2	3	6	25	39	69	152	502
Area	6	11	27	107	164	275	533	1185
Mean slope	2	3	7	30	48	84	183	582
Maximum slope	2	4	10	43	67	118	251	734

4.5. Comparison of the remotely sensed and field-based parameters of the sorted nets

The remotely sensed length and width of the sorted nets of 4.08 ± 1.02 m and 2.83 ± 0.75 m, respectively, differ on average by 0.06 m (1.6 %) and −0.43 m (−13.2 %) from the values obtained by the field surveys, which are 4.02 ± 0.83 m and 3.26 ± 0.76 m, respectively (Fig. 13). The length-to-width ratio of the remotely sensed sorted nets is 1.47 ± 0.28 compared with its field-based value of 1.26 ± 0.22. A good match between the remotely sensed and field-based parameters is for the diameter of the sorted nets (Fig. 13), which equals 3.46 ± 0.83 m and 3.64 ± 0.75 m, respectively, corresponding to a mean difference of −0.18 m (−4.9 %). On the other hand, the height of the remotely sensed sorted nets is 0.28 ± 0.10 m, while the height of those measured in the field is 0.43 ± 0.11 m, which results in a mean difference of −0.15 m (−34.9 %) (Fig. 13). The variability of the remotely sensed and field-based parameters of the sorted nets is similar, except for the length, the standard deviations of which differ by 0.19 m. The parameters also show the same types of probability distributions for both datasets (Fig. 13).

The sorting depth of 0.94 ± 0.22 m (Table 1) estimated from the remotely sensed diameter of the sorted nets is generally consistent with the sorting depth inferred from the ERT survey, which ranged ~0.5–1.8 m (Fig. 14). The ERT-based sorting depth also tends to increase with the diameter of the sorted nets.

5. Discussion

5.1. Mapping of the sorted nets

The DEM-derived rasters and aerial photographs with a horizontal resolution of 0.5 m and 0.2 m, respectively, used in this study (Fig. 3) proved to be sufficiently detailed to identify and delineate most of the sorted nets (Fig. 5). Poorly discernible patterns, however, occurred locally, which was probably due to their too small diameters and/or narrow troughs compared with the resolution of the remotely sensed

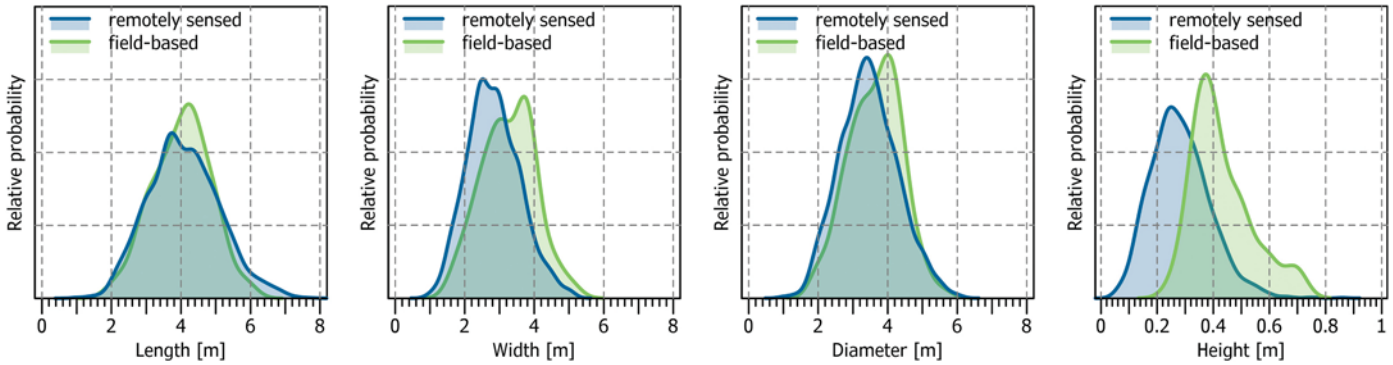

Fig. 13. Comparison of probability density of the basic remotely sensed and field-based parameters of the sorted nets.

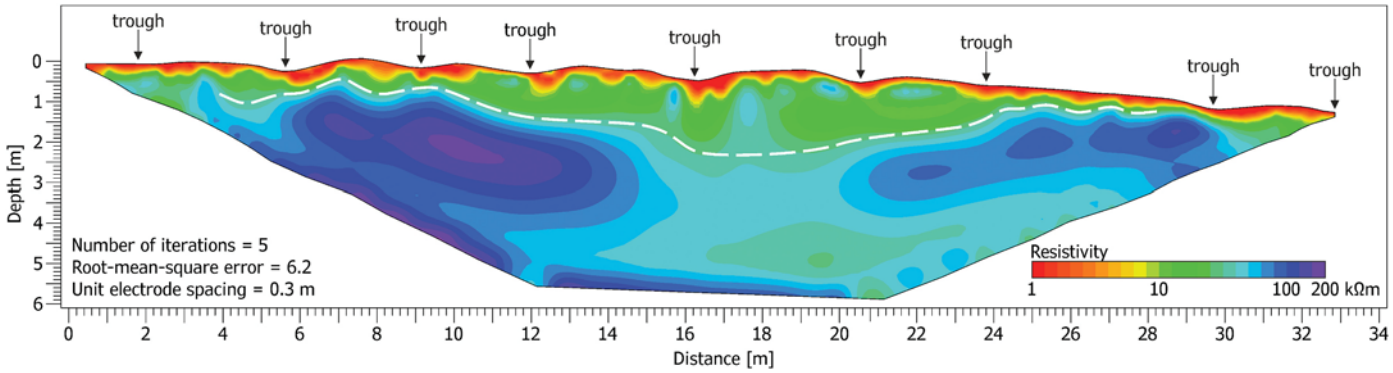

Fig. 14. Electrical resistivity tomogram from the study site intersecting eight complete sorted nets delineated by their bordering troughs. The white dashed line indicates the presumed sorting depth.

datasets, subdued relief of those sorted nets, and/or poor colour contrasts between their centres and troughs. The main sources of uncertainty are therefore potential errors in the identification of the troughs bordering the sorted nets and in the determination of the positions of the trough centrelines introduced by the manual vectorization, which is purely interpreter-dependent and inherently subjective. Nonetheless, this is no different from conventional field mapping. Several pilot studies have attempted to address this issue through fully- or semi-automatic detection and/or delineation tools using remotely sensed DEMs and aerial photographs, which had higher resolution than in this study and were collected specifically for that purpose (e.g., Abolt et al., 2019; Mather et al., 2019; Pereira et al., 2020; Zhang et al., 2018, 2020). However, these procedures are still being tested and may show errors of up to tens of percent for well-developed active patterned ground (Abolt et al., 2019; Pereira et al., 2020; Zhang et al., 2018, 2020) and are likely to be even less effective for relict one with subdued relief and/or vegetation cover (Mather et al., 2019). Consequently, we believe that, given the available datasets, the double-checked manual vectorization is currently more viable for accurately mapping the sorted nets examined in this study, albeit it is considerably time consuming.

5.2. Geometry of the sorted nets

The mean remotely sensed length, width, and diameter of the sorted nets showed the difference of 0.06 m (1.6 %), −0.43 m (−13.2 %), and −0.18 m (−4.9 %), respectively, from their field-based values measured at the same study site (Křížek et al., 2007, 2010, 2019; Treml et al., 2010). Given the horizontal resolution of the DEM and aerial photographs of 0.5 m and 0.2 m, respectively, this is better than expected, especially for the length and diameter. This is likely due to the large number of the remotely sensed sorted nets, which compensated for random errors and converged the parameters to their true values (Table 3). On the other hand, the remotely sensed length and width of the sorted nets were longer and shorter, respectively, than the field-based ones (Fig. 13). Likewise, the mean remotely sensed height of the sorted nets differed by −0.15 m (−34.9 %) from the field observations (Křížek et al., 2007, 2010, 2019; Treml et al., 2010). This relates to the horizontal resolution of the DEM of 0.5 m that smoothed the relief of the sorted nets and caused an undervaluation of the maximum elevation of their centres and, in particular, an overvaluation of the minimum elevation of their troughs, as the latter are typically no more than a few decimetres wide. Since the mean slope and maximum slope of the sorted nets highly depend on the pattern height (Table 2), these parameters are likely affected by the horizontal resolution of the DEM to a similar extent as the height. The vertical accuracy of the DEM probably has minor effect on the overall statistics of these parameters because we suppose that it is the same throughout the study site and that the uncertainties are random. We also suspect that the vertical accuracy of the DEM is actually much better than 0.18 m, as the difference between the remotely sensed and field-based height of the sorted nets is only −0.15 m, even though the DEM has a horizontal resolution of 0.5 m and the mean diameter of the sorted nets is <3.5 m.

The above suggests that purposively collected DEMs and/or aerial photographs with extremely high horizontal resolution in the order of centimetres to a few decimetres acquired using terrestrial devices or unmanned aerial vehicles, which have frequently been employed for sorted patterned ground (e.g., Dąbski et al., 2017; Mather et al., 2019; Pereira et al., 2020), are not necessary for reliable mapping and analysis of the horizontal geometry of patterns as large as those examined in this study. On the other hand, higher-resolution DEMs would be needed to better capture the relief of sorted patterned ground and to determine its vertical parameters, such as height and mean or maximum slope, more accurately than is now possible using manned aircrafts or satellites. Notwithstanding that, we believe that the relations between the

parameters of the sorted nets (Table 2) are generally valid because they are in line with sparse field observations on both active (e.g., Grab, 1997; Holness, 2003; Uxa et al., 2017) and relict (e.g., Grab, 2002; Křížek and Uxa, 2013) sorted patterned ground.

The sorting depth of 0.94 ± 0.22 m (Table 1) estimated from the remotely sensed diameter of the sorted nets is also plausible because it is consistent with the sorting depth determined by the ERT survey (Fig. 14) and with values previously published from the same study site and other locations in the Krkonoše Mts. based on excavations, which were typically ~0.4–1.0 m (Kunský and Záruba, 1950; Sekyra, 1960; Sekyra and Sekyra, 1995; Sekyra et al., 2002) and the deepest ones achieved up to 1.5–2.0 m (Králík and Sekyra, 1969; Engel et al., 2021). Likewise, the diameter-to-sorting depth ratios of the sorted nets defined by the Eq. (2) (Fig. 6) are close to those that can be derived from cross-section sketches for several relict sorted patterns in the Krkonoše Mts. as well as for active sorted patterned ground from other regions (Fig. 15). Although the variability of the sorting depth may seem high (Table 1; Fig. 9), its coefficient of variation of 0.24 is not far from its typical value of 0.17 ± 0.09 that can be inferred from other publications on sorted patterned ground (Warburton, 1987; Warburton and Caine, 1999; Boelhouwers et al., 2003; Holness, 2003) (Fig. 16). This indicates that the probability distribution of the sorting depth can be reasonably estimated from the remotely sensed sorted patterned ground while overcoming two major shortcomings of field surveys. Firstly, numerous excavations would be required if the probability distribution of the sorting depth was to be determined directly, which would be extremely laborious and in reality impossible at the study site because it is under the highest level of nature protection and excavations are now outlawed there. Secondly, the sorting depth may be difficult to determine accurately even in excavations, and if not, it may have changed due to millennial degradation of the sorted nets. On the other hand, we believe that their horizontal parameters, on the basis of which the sorting depth was estimated in this study, have been largely retained since the sorted nets were last active

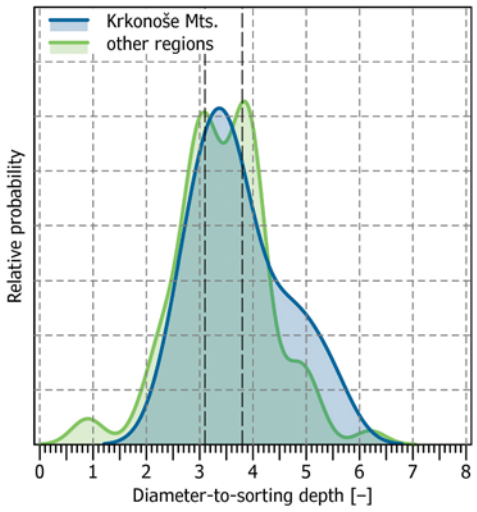

Fig. 15. Comparison of probability density of diameter-to-sorting depth ratios based on twelve values for relict sorted patterned ground in the Krkonoše Mts. (Sekyra, 1960; Sekyra and Sekyra, 1995; Sekyra et al., 2002) and seventy-five values for active sorted patterned ground from other regions (Troll, 1944; Furrer, 1955; Sekyra, 1969; Bunting and Jackson, 1970; Freund, 1971; Graf, 1973; Ellenberg, 1976; Ballantyne and Matthews, 1982; Ray et al., 1983; Gleason et al., 1986; Hallet and Prestrud, 1986; Walters, 1988; Cook, 1989; Van Vliet-Lanoë, 1991; Wilson and Clark, 1991; Wilson, 1992; Ballantyne and Harris, 1994; Kück, 1996; Grab, 1997; Kling, 1997; Humlum and Christiansen, 1998; Holness, 2003; Dąbski, 2005; Uxa et al., 2017). The vertical black dashed lines indicate the theoretical range of the diameter-to-sorting depth ratio of ~3.1–3.8 (Ray et al., 1983; Gleason et al., 1986; Hallet and Prestrud, 1986; Krantz, 1990).

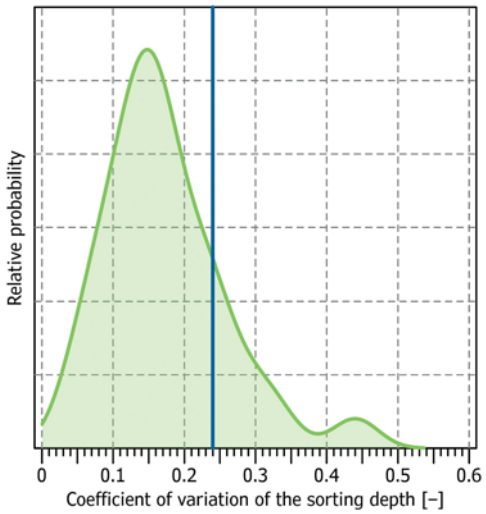

Fig. 16. Probability density of coefficient of variation of the sorting depth inferred from published values at thirty-one sites with active sorted patterned ground (Warburton, 1987; Warburton and Caine, 1999; Boelhouwers et al., 2003; Holness, 2003). The blue vertical line represents the coefficient of variation of the sorting depth of 0.24 determined at the study site.

(sensu Hallet and Prestrud, 1986; Kessler et al., 2001; Peterson and Krantz, 2008).

Other parameters of the sorted nets and their relationships cannot be evaluated properly because they are difficult to determine by field measurements, and therefore have also hardly been investigated for any sorted patterned ground. Yet, the number of sides and side inner angles of the sorted nets of 5.99 ± 1.13 and 119.9 ± 25.6°, respectively (Table 1), are consistent with sparse field data and theoretical predictions on polygonal sorted patterned ground, which also peaked at six sides and side inner angles of ~120° mostly forming three-way junctions (Ray et al., 1983; Gleason et al., 1986; Kessler and Werner, 2003). Similar values have also been found for active (e.g., Lousada et al., 2018; Frappier and Lacelle, 2021) and relict (e.g., Bertran, 2022) thermal-contraction-cracking polygons. The pronounced rightward skew of the area of the sorted nets (Fig. 9) is consistent with sparse field data and theoretical predictions (Kessler and Werner, 2003), and is characteristic for many tessellated systems found in nature (Pineda et al., 2004; Xu and Li, 2009). Likewise, the skew of some of the other parameters of the sorted nets (Fig. 9) has been observed before, but usually much larger than in this study (e.g., Ballantyne and Matthews, 1982; Francou et al., 2001; Uxa et al., 2017). However, the latter observations may have been affected by the fact that they were based on samples from multiple sites with variable environmental conditions (Francou et al., 2001; Uxa et al., 2017) or sorted patterns of different ages (Ballantyne and Matthews, 1982).

5.3. *Palaeo-environmental and methodological implications of the study*

Sorted nets over 1 m in diameter are thought to form under the mean annual air temperature below −6 °C to −4 °C and in the presence of continuous permafrost (Goldthwait, 1976; Washburn, 1980; Grab, 2002; Ballantyne, 2013, 2018). Hence, the mean annual air temperature at the study site is estimated to have been reduced by at least ~5–7 °C or ~6–8 °C during the Last Glacial Maximum, when the sorted nets presumably developed (cf. Engel et al., 2021), compared to 1961–1990 or 1981–2010, respectively. However, it must be stressed that this is a minimum estimate, and indeed a slightly more pronounced decline in the mean annual air temperature of at least ~6–10 °C or ~7–11 °C compared to 1961–1990 or 1981–2010, respectively, has been suggested previously for the summit area of the Krkonoše Mts. (Heyman et al., 2013; Engel et al., 2021).

Since sorting depth is believed to be constrained by the freeze-thaw depth at the time of patterned-ground development (Hallet and Prestrud, 1986; Ballantyne and Harris, 1994), 0.94 ± 0.22 m thick active layer (Table 1) likely superimposed permafrost at the study site when the sorted nets formed. This is in line with previous suggestion of the Last Glacial Maximum active-layer thickness in the summit area of the Krkonoše Mts. of 1 m (Jahn, 1977) and similar estimates based on sorted polygons of 0.9–1.6 m (Engel et al., 2021). The knowledge of past active-layer thickness has a considerable palaeo-environmental importance because it can be further exploited for reconstructing past climate conditions (Uxa et al., 2021).

The collected dataset of the remotely sensed parameters of the sorted nets is also valuable for choosing an effective sample size for individual parameters as well as for deciding on the minimum network size to be included in statistical comparisons of multiple polygonal networks because we showed that most of the parameters can be typically determined with the absolute percentage error constantly below 10 % and 5 % of the mean parameter value (for instance ~0.35 m and ~0.17 m, respectively, for the diameter of the sorted nets) already at ~30 and ~30–100 observations, respectively (Table 3). Obviously, the number of observations required could be affected by spatial variations of the parameters of the sorted nets, but these are not related to elevation or slope inclination, which is due to the relatively small extent of the study site (~1.79 ha) and its flat and homogeneous topography. Consequently, we believe that our analysis is robust and could be a useful guide for increasing the effectivity and credibility of future remotely sensed as well as field surveys of polygonal networks of similar appearance and topographic context. Likewise, the knowledge of the probability distributions of the individual parameters of the sorted nets (Fig. 9) has important implications for the proper statistical treatment of their limited samples, which may be so small that their probability distributions cannot be reliably determined.

Lastly, the collected dataset of the remotely sensed parameters of the sorted nets can also be used to evaluate the accuracy of automated mapping and/or delineation tools for sorted patterned ground (e.g., Mather et al., 2019; Pereira et al., 2020), which should definitely be developed further because they can considerably reduce the time required for the digitization and supress its subjectivity. Similarly, the dataset can be used to test the models of patterned-ground growth, as comprehensive datasets of pattern parameters, on which the models could be tested, are not yet available.

6. Conclusions

Sorted patterned ground is an abundant feature in past and present periglacial landscapes, but has so far been investigated mostly by field methods. We demonstrated that the region-wide high-resolution DEM and aerial photographs with a horizontal resolution of 0.5 m and 0.2 m, respectively, allow to reliably map and analyse large sets of last glacial sorted nets and to determine many of their geometric parameters, which would be difficult in conventional field surveys. Basic remotely sensed parameters such as the length, width, and diameter of the sorted nets differ by less than ~13 % from the field-based values measured at the same study site, whereas the height is ~35 % lower. Most remotely sensed parameters of the sorted nets typically require ~30–100 observations for the absolute percentage error to be constantly below 5 % of the mean parameter value. It can be expected that a higher-resolution DEM would further reduce both the deviations and the number of observations needed. Besides that, the remotely sensed diameter of the sorted nets can also be used to estimate the thickness of the past active layer over permafrost, which was nearly 1 m at the study site during the Last Glacial Maximum and the mean annual air temperature likely declined by at least ~5–8 °C compared to the modern climate. Consequently, remote sensing of sorted patterned ground can aid in past permafrost and climate modelling.

Similar manually collected parameter datasets should be further used to validate automated mapping and/or delineation tools for sorted patterned ground, thereby allowing its digitization over extensive areas with less time and less subjectivity. This could bring a wealth of new information on sorted patterned ground and its characteristics from past and present periglacial landscapes, which is important for refining its environmental limits as well as for enhancing its relevance as an indicator of past permafrost and climate states. The collected datasets could also be used to test the models of patterned-ground growth, which are essential for better understanding the long-term dynamics of sorted patterned ground and its environmental feedbacks.

CRediT authorship contribution statement

Tomáš Uxa: Conceptualization, Methodology, Software, Validation, Formal analysis, Investigation, Data curation, Writing – original draft, Visualization. **Marek Křížek:** Conceptualization, Methodology, Investigation, Writing – review & editing, Supervision, Funding acquisition. **Tereza Dlabáčková:** Investigation, Writing – review & editing. **David Krause:** Investigation, Resources, Writing – review & editing.

Declaration of competing interest

The authors declare that they have no known competing financial interests or personal relationships that could have appeared to influence the work reported in this paper.

Data availability

A supplementary file with the geometric parameters of the remotely sensed sorted nets is released along with the manuscript. All other data collected are available from the corresponding author upon reasonable request.

Acknowledgements

This work was supported by the Czech Science Foundation [grant number 21-23196S]. The Krkonoše Mountains National Park Administration is thanked for permission to carry out research in a strictly protected area. We thank two anonymous reviewers for comments and suggestions on an earlier version of the manuscript.

Appendix A. Supplementary data

Supplementary data to this article can be found online at https://doi.org/10.1016/j.geomorph.2023.108615.

References

Abolt, C.J., Young, M.H., Atchley, A.L., Wilson, C.J., 2019. Brief communication: rapid machine-learning-based extraction and measurement of ice wedge polygons in high-resolution digital elevation models. Cryosphere 13, 237–245. https://doi.org/10.5194/tc-13-237-2019.

Anderson, K., Westoby, M.J., James, M.R., 2019. Low-budget topographic surveying comes of age: structure from motion photogrammetry in geography and the geosciences. Prog. Phys. Geogr. 43, 163–173. https://doi.org/10.1177/0309133319837454.

Andrieux, E., Bertran, P., Saito, K., 2016. Spatial analysis of the French Pleistocene permafrost by a GIS database. Permafr. Periglac. Process. 27, 17–30. https://doi.org/10.1002/ppp.1856.

Ballantyne, C.K., 2013. Patterned ground. In: Elias, S.A., Mock, C.J. (Eds.), Encyclopedia of Quaternary Science, 2nd edition. Elsevier, Amsterdam, pp. 452–463.

Ballantyne, C.K., 2018. Periglacial Geomorphology. John Wiley & Sons, Hoboken.

Ballantyne, C.K., Harris, C., 1994. The Periglaciation of Great Britain. Cambridge University Press, Cambridge.

Ballantyne, C.K., Matthews, J.A., 1982. The development of sorted circles on recently deglaciated terrain, Jotunheimen, Norway. Arctic Alpine Res. 14, 341–354. https://doi.org/10.1080/00040851.1982.12004316.

Beerten, K., Meylemans, E., Kasse, C., Mestdagh, T., Van Rooij, D., Bastiaens, J., 2021. Networks of unusually large fossil periglacial polygons, Campine area, northern Belgium. Geomorphology 377, 107582. https://doi.org/10.1016/j.geomorph.2020.107582.

Bernard-Grand'Maison, C., Pollard, W., 2018. An estimate of ice wedge volume for a High Arctic polar desert environment, Fosheim Peninsula, Ellesmere Island. Cryosphere 12, 3589–3604. https://doi.org/10.5194/tc-12-3589-2018.

Berthling, I., Berti, C., Mancinelli, V., Stendardi, L., Piacentini, T., Miccadei, E., 2020. Analysis of the paraglacial landscape in the Ny-Ålesund area and Blomstrandøya (Kongsfjorden, Svalbard, Norway). J. Maps 16, 818–833. https://doi.org/10.1080/17445647.2020.1837684.

Bertran, P., 2022. Distribution and characteristics of Pleistocene ground thermal contraction polygons in Europe from satellite images. Permafr. Periglac. Process. 33, 99–113. https://doi.org/10.1002/ppp.2137.

Bhuiyan, M.A.E., Witharana, C., Liljedahl, A.K., 2020. Use of very high spatial resolution commercial satellite imagery and deep learning to automatically map ice-wedge polygons across tundra vegetation types. J. Imaging 6, 137. https://doi.org/10.3390/jimaging6120137.

Boelhouwers, J., Holness, S., Sumner, P., 2003. The maritime subantarctic: a distinct periglacial environment. Geomorphology 52, 39–55. https://doi.org/10.1016/S0169-555X(02)00247-7.

Bunting, B.T., Jackson, R.H., 1970. Studies of patterned ground on SW Devon Island, NWT: a method for collecting undisturbed megasamples from dry arctic polygons and observations on some physical properties of the material in a sorted polygon. Geogr. Ann. A: Phys. Geogr. 52, 194–208. https://doi.org/10.1080/04353676.1970.11879824.

Chaloupský, J., Červenka, J., Jetel, J., Králík, F., Líbalová, J., Píchová, E., Pokorný, J., Pošmourný, K., Sekyra, J., Shrbený, O., Šamanský, K., Šrámek, J., Václ, J., 1989. Geologie Krkonoš a Jizerských hor (Geology of the Krkonoše and Jizerské hory Mts.) (in Czech). Academia, Prague.

Chiasson, A., Allard, M., 2022. Thermal contraction crack polygons in Nunavik (northern Quebec): distribution and development of polygonal patterned ground. Permafr. Periglac. Process. 33, 195–213. https://doi.org/10.1002/ppp.2150.

Chlupáč, I., Brzobohatý, R., Kovanda, J., Stráník, Z., 2011. Geologická minulost České republiky (Geological History of the Czech Republic) (in Czech), 2nd edition. Academia, Prague.

Cook, J.D., 1989. Active and Relict Sorted Circles, Jotunheimen, Norway: A Study of the Altitudinal Zonation of Periglacial Processes. University of Wales, Cardiff. PhD thesis.

Coufal, L., Míková, T., Langová, P., 1992. Meteorologická data na území ČR za období 1961–90 (Meteorological data on the territory of the Czech Republic for the period 1961–90) (in Czech). Nakladatelství Českého hydrometeorologického ústavu, Prague.

Czudek, T., 2005. Vývoj reliéfu krajiny České republiky v kvartéru (Quaternary development of landscape relief of the Czech Republic) (in Czech). Moravské zemské museum, Brno.

Dąbski, M., 2005. Small-scale sorted nets on Glacial Till, Fláajökull (Southeast Iceland) and Elisbreen (Northwest Spitsbergen). Permafr. Periglac. Process. 16, 305–310. https://doi.org/10.1002/ppp.527.

Dąbski, M., Zmarz, A., Pabjanek, P., Korczak-Abshire, M., Karsznia, I., Chwedorzewska, K.J., 2017. UAV-based detection and spatial analyses of periglacial landforms on Demay Point (King George Island, South Shetland Islands, Antarctica). Geomorphology 290, 29–38. https://doi.org/10.1016/j.geomorph.2017.03.033.

Delignette-Muller, M.L., Dutang, C., 2015. fitdistrplus: an R package for fitting distributions. J. Stat. Softw. 64, 1–34. https://doi.org/10.18637/jss.v064.i04.

Ellenberg, L., 1976. Rezente Periglazialerscheinungen auf Cheju Dô, Südkorea (Recent periglacial phenomena on Cheju Dô, South Korea) (in German). Geogr. Helv. 31, 69–74. https://doi.org/10.5194/gh-31-69-1976.

Engel, Z., Braucher, R., Traczyk, A., Laetitia, L., ASTER team, 2014. ^{10}Be exposure age chronology of the last glaciation in the Krkonoše Mountains, Central Europe. Geomorphology 206, 107–121. https://doi.org/10.1016/j.geomorph.2013.10.003.

Engel, Z., Křížek, M., Braucher, R., Uxa, T., Krause, D., AsterTeam, 2021. ^{10}Be exposure age for sorted polygons in the Sudetes Mountains. Permafr. Periglac. Process. 32, 154–168. https://doi.org/10.1002/ppp.2091.

Evans, D.J.A., Kalyan, R., Orton, C., 2017. Periglacial geomorphology of summit tors on Bodmin Moor, Cornwall, SW England. J. Maps 13, 342–349. https://doi.org/10.1080/17445647.2017.1308283.

Ewertowski, M.W., Kijowski, A., Szuman, I., Tomczyk, A.M., Kasprzak, L., 2017. Low-altitude remote sensing and GIS-based analysis of cropmarks: classification of past thermal-contraction-crack polygons in central western Poland. Geomorphology 293, 418–432. https://doi.org/10.1016/j.geomorph.2016.07.022.

Feuillet, T., Mercier, D., Decaulne, A., Cossart, E., 2012. Classification of sorted patterned ground areas based on their environmental characteristics (Skagafjörður, Northern Iceland). Geomorphology 139–140, 577–587. https://doi.org/10.1016/j.geomorph.2011.12.022.

Francou, B., Méhauté, N.L., Jomelli, V., 2001. Factors controlling spacing distances of sorted stripes in a low-latitude, alpine environment (Cordillera Real, 16° S, Bolivia). Permafr. Periglac. Process. 12, 367–377. https://doi.org/10.1002/ppp.398.

Frappier, R., Lacelle, D., 2021. Distribution, morphometry, and ice content of ice-wedge polygons in Tombstone Territorial Park, central Yukon,Canada. Permafr. Periglac. Process. 32, 587–600. https://doi.org/10.1002/ppp.2123.

Freund, R., 1971. Die Kleinformen der Frostmusterböden: Vergleich Arktis – Alpen - Tropisches Hochgebirge (Small-scale Patterned Ground: Comparison of Arctic - Alps - Tropical High Moutains) (in German). Geogr. Helv. 26, 142–147. https://doi.org/10.5194/gh-26-142-1971.

Furrer, G., 1955. Die Strukturbodenformen der Alpen. (Patterned ground of the Alps) (in German). Geogr. Helv. 10, 193–213. https://doi.org/10.5194/gh-10-193-1955.

Gleason, K.J., Krantz, W.B., Caine, N., George, J.H., Gunn, R.D., 1986. Geometrical aspects of sorted patterned ground in recurrently frozen soil. Science 232, 216–220. https://doi.org/10.1126/science.232.4747.216.

Goldthwait, R.P., 1976. Frost sorted patterned ground: a review. Quat. Res. 6, 27–35. https://doi.org/10.1016/0033-5894(76)90038-7.

Grab, S.W., 1997. Annually re-forming miniature sorted patterned ground in the High Drakensberg, southern Africa. Earth Surf. Process. Landf. 22, 733–745. https://doi.org/10.1002/(SICI)1096-9837(199708)22:8<733::AID-ESP764>3.0.CO;2-L.

Grab, S., 2002. Characteristics and palaeoenvironmental significance of relict sorted patterned ground, Drakensberg plateau, southern Africa. Quat. Sci. Rev. 21, 1729–1744. https://doi.org/10.1016/S0277-3791(01)00149-4.

Graf, K., 1973. Vergleichende Betrachtungen zur Solifluktion in verschiedenen Breitenlagen (Comparative considerations on solifluction in different latitudes) (in German). Z. Geomorphol. Suppl. 16, 104–154.

Groos, A.R., Niederhauser, J., Wraase, L., Hänsel, F., Nauss, T., Akçar, N., Veit, H., 2021. The enigma of relict large sorted stone stripes in the tropical Ethiopian Highlands. Earth Surf. Dyn. 9, 145–166. https://doi.org/10.5194/esurf-9-145-2021.

Hallet, B., 2013. Stone circles: form and soil kinematics. Philos. Trans. R. Soc. A 371, 20120357. https://doi.org/10.1098/rsta.2012.0357.

Hallet, B., Prestrud, S., 1986. Dynamics of periglacial sorted circles in Western Spitsbergen. Quat. Res. 26, 81–99. https://doi.org/10.1016/0033-5894(86)90085-2.

Haltigin, T.W., Pollard, W.H., Dutilleul, P., Osinski, G.R., 2012. Geometric evolution of polygonal terrain networks in the Canadian High Arctic: evidence of increasing regularity over time. Permafr. Periglac. Process. 23, 178–186. https://doi.org/10.1002/ppp.1741.

Harčarik, J., 2002. Microclimatic relationships of the arctic-alpine tundra. Opera Corcontica 39, 45–68.

Harris, S.A., Brouchkov, A., Guodong, C., 2018. Geocryology. Characteristics and Use of Frozen Ground and Permafrost Landforms. CRC Press, Taylor & Francis Group, London.

Heyman, B.M., Heyman, J., Fickert, T., Harbor, J.M., 2013. Paleo-climate of the central European uplands during the last glacial maximum based on glacier mass-balance modeling. Quat. Res. 79, 49–54. https://doi.org/10.1016/j.yqres.2012.09.005.

Holness, S.D., 2003. Sorted circles in the maritime Subantarctic, Marion Island. Earth Surf. Process. Landf. 28, 337–347. https://doi.org/10.1002/esp.430.

Humlum, O., Christiansen, H.H., 1998. Mountain climate and periglacial phenomena in the Faeroe Islands. Permafr. Periglac. Process. 9, 189–211. https://doi.org/10.1002/(SICI)1099-1530(199807/09)9:3<189::AID-PPP287>3.0.CO;2-N.

Jahn, A., 1977. The permafrost active layer in the Sudety Mountains during the last glaciation. Quaest. Geogr. 4, 29–42.

Kääb, A., Girod, L., Berthling, I., 2014. Surface kinematics of periglacial sorted circles using structure-from-motion technology. Cryosphere 8, 1041–1056. https://doi.org/10.5194/tc-8-1041-2014.

Kessler, M.A., Werner, B.T., 2003. Self-organization of sorted patterned ground. Science 299, 380–383. https://doi.org/10.1126/science.1077309.

Kessler, M.A., Murray, A.B., Werner, B.T., 2001. A model for sorted circles as self-organized patterns. J. Geophys. Res.: SolidEarth 106, 13287–13306. https://doi.org/10.1029/2001JB000279.

Kling, J., 1997. Observations on sorted circle development, Abisko, Northern Sweden. Permafr. Periglac. Process. 8, 447–453. https://doi.org/10.1002/(SICI)1099-1530(199710/12)8:4<447::AID-PPP266>3.0.CO;2-H.

Kociánová, M., Sekyra, J., 1995. Distribution of vegetated patterned grounds. In: Soukupová, L., Kociánová, M., Jeník, J., Sekyra, J. (Eds.), Arctic-alpine Tundra in the Krkonoše, the Sudetes. Opera Corcontica, 32, pp. 54–66.

Králík, F., Sekyra, J., 1969. Geomorfologický přehled Krkonoš (Geomorphological overview of the Krkonoše Mts.) (in Czech). In: Fanta, J. (Ed.), Příroda Krkonošského národního parku, Státní zemědělské nakladatelství, Prague, pp. 59–87.

Krantz, W.B., 1990. Self-organization manifest as patterned ground in recurrently frozen soils. Earth-Sci. Rev. 29, 117–130. https://doi.org/10.1016/0012-8252(0)90031-P.

Krause, D., Fišer, J., Křížek, M., 2022. Morphological differences of longitudinal profiles between glacial cirques and non-glacial valley heads, described by mathematical fitting. Geomorphology 404, 108183. https://doi.org/10.1016/j.geomorph.2022.108183.

Křížek, M., 2007. Periglacial landforms above the alpine timberline in the High Sudetes. In: Goudie, A.S., Kalvoda, J. (Eds.), Geomorphological Variations. P3K, Prague, pp. 313–337.

Křížek, M., Uxa, T., 2013. Morphology, sorting and microclimates of relict sorted polygons, Krkonoše Mountains, Czech Republic. Permafr. Periglac. Process. 24, 313–321. https://doi.org/10.1002/ppp.1789.

Křížek, M., Treml, V., Engel, Z., 2007. Litologická predispozice, morfologie a rozmístění strukturních půd alpinského bezlesí Vysokých Sudet (Lithologic predisposition, morphology, and spatial distribution of patterned ground above alpine timberline in the High Sudetes) (in Czech). Geogr.-Sb. CGS 112, 373–382. https://doi.org/10.37040/geografie2007112040373.

Křížek, M., Treml, V., Engel, Z., 2010. Czy najwyższe partie Sudetów powyżej górnej granicy lasu są domeną peryglacjalną? (Are the highest parts of the Sudetes above timberline the periglacial domain?) (in Polish). Czasopismo Geograficzne 81, 75–102.

Křížek, M., Vočadlová, K., Engel, Z., 2012. Cirque overdeepening and their relationship to morphometry. Geomorphology 139–140, 495–505. https://doi.org/10.1016/j.geomorph.2011.11.014.

Křížek, M., Krause, D., Uxa, T., Engel, Z., Treml, T., Traczyk, A., 2019. Patterned ground above the alpine timberline in the High Sudetes, Central Europe. J. Maps 15, 563–569. https://doi.org/10.1080/17445647.2019.1636890.

Kück, K.M., 1996. Periglacial Features in the Vicinity of Tiffindell Ski Resort, North East Cape Drakensberg, South Africa, and Their Implications for the Development of the Resort. Rhodes University, Grahamstown. PhD thesis.

Kunský, J., Záruba, Q., 1950. Periglaciální strukturní půdy v Krkonoších (The Periglacial Structural Soils in the Giants Mountains) (in Czech). Geogr.-Sb. CGS 10–14.
Lousada, M., Pina, P., Vieira, G., Bandeira, L., Mora, C., 2018. Evaluation of the use of very high resolution aerial imagery for accurate ice-wedge polygon mapping (Adventdalen, Svalbard). Sci. Total Environ. 615, 1574–1583. https://doi.org/10.1016/j.scitotenv.2017.09.153.
Mather, A.E., Fyfe, R.M., Clason, C.C., Stokes, M., Mills, S., Barrows, T.T., 2019. Automated mapping of relict patterned ground: an approach to evaluate morphologically subdued landforms using unmanned-aerial-vehicle and structure-from-motion technologies. Prog. Phys. Geogr. 43, 174–192. https://doi.org/10.1177/0309133318788966.
Migała, K., Urban, G., Tomczyński, K., 2016. Long-term air temperature variation in the Karkonosze mountains according to atmospheric circulation. Theor. Appl. Climatol. 125, 337–351. https://doi.org/10.1007/s00704-015-1468-0.
Migoń, P., 1999. The role of 'preglacial' relief in the development of mountain glaciation in the Sudetes, with the special references to the Karkonosze Mountains. Z. Geomorphol. Suppl. 113, 33–44.
Pereira, F., Marques, J.S., Heleno, S., Pina, P., 2020. Detection and delineation of sorted stone circles in Antarctica. Remote Sens. 12, 160. https://doi.org/10.3390/rs12010160.
Peterson, R.A., Krantz, W.B., 2008. Differential frost heave model for patterned ground formation: corroboration with observations along a North American arctic transect. J. Geophys.Res. Biogeosci. 113, G03S04. https://doi.org/10.1029/2007JG000559.
Pineda, E., Bruna, P., Crespo, D., 2004. Cell size distribution in random tessellations of space. Phys. Rev. E 70, 066119. https://doi.org/10.1103/PhysRevE.70.066119.
Ping, C.L., Jastrow, J.D., Jorgenson, M.T., Michaelson, G.J., Shur, Y.L., 2015. Permafrost soils and carbon cycling. Soil 1, 147–171. https://doi.org/10.5194/soil-1-147-2015.
Pińskwar, I., Choryński, A., Graczyk, D., Kundzewicz, Z.W., 2019. Observed changes in precipitation totals in Poland. Geogr.-Sb. CGS 124, 237–264. https://doi.org/10.37040/geografie2019124030237.
Puchrik, L., Nýdrle, J., 2013. Snímkování a letecké laserové skenování Krkonošského národního parku (Imaging and aerial laser scanning of the Krkonoše Mts. National Park) (in Czech). Geodis News 12, 24.
Ray, R.J., Krantz, W.B., Caine, T.N., Gunn, R.D., 1983. A model for sorted patterned-ground regularity. J. Glaciol. 29, 317–337. https://doi.org/10.3198/1983JoG29-102-317-337.
Rettelbach, T., Langer, M., Nitze, I., Jones, B., Helm, V., Freytag, J.C., Grosse, G., 2021. A quantitative graph-based approach to monitoring ice-wedge trough dynamics in polygonal permafrost landscapes. Remote Sens. 13, 3098. https://doi.org/10.3390/rs13163098.
Sekyra, J., 1960. Působení mrazu na půdu: Kryopedologie se zvláštním zřetelem k ČSR (Effects of frost on soil: Cryopedology with special emphasis on Czechoslovakia) (in Czech). Nakladatelství Československé akademie věd, Prague.
Sekyra, J., 1969. Profil polygonálními strukturami na středněpleistocenní moréně (Profile through polygonal patterns on a middle Pleistocene moraine) (in Czech). In: Černík, A., Sekyra, J. (Eds.), Zeměpis velehor. Nakladatelství Československé akademie věd, Prague, p. 29.
Sekyra, J., Sekyra, Z., 1995. Recent cryogenic processes. In: Soukupová, L., Kociánová, M., Jeník, J., Sekyra, J. (Eds.), Arctic-alpine Tundra in the Krkonoše, the Sudetes. Opera Corcontica, 32, pp. 31–37.
Sekyra, J., Kociánová, M., Šturmová, H., Dvořák, I.J., Svoboda, M., 2002. Frost phenomena in relationship to mountain pine. Opera Corcontica 39, 69–114.
Smith, M.J., Pain, C.F., 2009. Applications of remote sensing in geomorphology. Prog. Phys. Geogr. 33, 568–582. https://doi.org/10.1177/0309133309346648.
Smith, M.W., Carrivick, J.L., Quincey, D.J., 2016. Structure from motion photogrammetry in physical geography. Prog. Phys. Geogr. 40, 247–275. https://doi.org/10.1177/0309133315615805.
Traczyk, A., 2004. Late Pleistocene evolution of periglacial and glacial relief in the Karkonosze Mountains: new hypotheses and research perspectives. Acta Univ. Carol. Geogr. 39, 59–72.
Traczyk, A., Migoń, P., 2000. Cold-climate landform patterns in the Sudetes. Effects of lithology, relief and glacial history. Acta Univ. Carol. Geogr. 35, 185–210.
Treml, V., Jankovská, V., Petr, L., 2008. Holocene dynamics of the alpine timberline in the High Sudetes. Biologia 63, 73–80. https://doi.org/10.2478/s11756-008-0021-3.
Treml, V., Křížek, M., Engel, Z., 2010. Classification of patterned ground based on morphometry and site characteristics: a case study from the High Sudetes, Central Europe. Permafr. Periglac. Process. 21, 66–77. https://doi.org/10.1002/ppp.671.
Troll, C., 1944. Strukturböden, Solifluktion und Frostklimate der Erde (Patterned ground, Solifluction, and Frost Climates of the Earth) (in German). Geol. Rundsch. 34, 545–694. https://doi.org/10.1007/BF01803103.
Uxa, T., Mida, P., Křížek, M., 2017. Effect of climate on morphology and development of sorted circles and polygons. Permafr. Periglac. Process. 28, 663–674. https://doi.org/10.1002/ppp.1949.
Uxa, T., Křížek, M., Hrbáček, F., 2021. PERICLIMv1.0: a model deriving palaeo-air temperatures from thaw depth in past permafrost regions. Geosci. Model Dev. 14, 1865–1884. https://doi.org/10.5194/gmd-14-1865-2021.
Van Vliet-Lanoë, B., 1991. Differential frost heave, load casting and convection: converging mechanisms; a discussion of the origin of cryoturbations. Permafr. Periglac. Process. 2, 123–139. https://doi.org/10.1002/ppp.3430020207.
Walker, D.A., Epstein, H.E., Romanovsky, V.E., Ping, C.L., Michaelson, G.J., Daanen, R. P., Shur, Y., Peterson, R.A., Krantz, W.B., Raynolds, M.K., Gould, W.A., Gonzalez, G., Nicolsky, D.J., Vonlanthen, C.M., Kade, A.N., Kuss, P., Kelley, A.M., Munger, C.A., Tarnocai, C.T., Matveyeva, N.V., Daniëls, F.J.A., 2008. Arctic patterned-ground ecosystems: a synthesis of field studies and models along a North American Arctic Transect. J. Geophys. Res.: Biogeosci. 113, G03S01 https://doi.org/10.1029/2007JG000504.
Walters, J.C., 1988. Observations of sorted patterned ground features, High Valley/Tangle Lakes region, Central Alaska, U.S.A. Z. Geomorphol. Suppl. 71, 93–106.
Warburton, J., 1987. Characteristic ratios of width to depth-of-sorting for sorted stripes in the English Lake District. In: Boardman, J. (Ed.), Periglacial Processes and Landforms in Britain and Ireland. Cambridge University Press, Cambridge, pp. 163–171.
Warburton, J., 2013. Patterned ground and polygons. In: Shroder, J., Giardino, R., Harbor, J. (Eds.), Treatise on Geomorphology, Glacial and Periglacial Geomorphology, Vol. 8. Academic Press, San Diego, pp. 298–312.
Warburton, J., Caine, N., 1999. Sorted patterned ground in the English Lake District. Permafr. Periglac. Process. 10, 193–197. https://doi.org/10.1002/(SICI)1099-1530(199904/06)10:2<193::AID-PPP291>3.0.CO;2-F.
Washburn, A.L., 1980. Permafrost features as evidence of climatic change. Earth-Sci. Rev. 15, 327–402. https://doi.org/10.1016/0012-8252(80)90114-2.
Wilson, P., 1992. Small-scale patterned ground, Comeragh Mountains, southeast Ireland. Permafr. Periglac. Process. 3, 63–70. https://doi.org/10.1002/ppp.3430030109.
Wilson, P., Clark, R., 1991. Development of miniature sorted patterned ground following soil erosion in East Falkland,South Atlantic. Earth Surf. Process. Landf. 16, 369–376. https://doi.org/10.1002/esp.3290160409.
Witharana, C., Bhuiyan, M.A.E., Liljedahl, A.K., Kanevskiy, M., Epstein, H.E., Jones, B. M., Daanen, R., Griffin, C.G., Kent, K., Jones, M.K.W., 2020. Understanding the synergies of deep learning and data fusion of multispectral and panchromatic high resolution commercial satellite imagery for automated ice-wedge polygon detection. ISPRS J. Photogramm. Remote Sens. 170, 174–191. https://doi.org/10.1016/j.isprsjprs.2020.10.010.
Witharana, C., Bhuiyan, M.A.E., Liljedahl, A.K., Kanevskiy, M., Jorgenson, T., Jones, B. M., Daanen, R., Epstein, H.E., Griffin, C.G., Kent, K., Ward Jones, M.K., 2021. An object-based approach for mapping tundra ice-wedge polygon troughs from very high spatial resolution optical satellite imagery. Remote Sens. 13, 558. https://doi.org/10.3390/rs13040558.
Xu, T., Li, M., 2009. Topological and statistical properties of a constrained Voronoi tessellation. Philos. Mag. 89, 349–374. https://doi.org/10.1080/14786430802647065.
Zhang, W., Witharana, C., Liljedahl, A.K., Kanevskiy, M., 2018. Deep convolutional neural networks for automated characterization of arctic ice-wedge polygons in very high spatial resolution aerial imagery. Remote Sens. 10, 1487. https://doi.org/10.3390/rs10091487.
Zhang, W., Liljedahl, A.K., Kanevskiy, M., Epstein, H.E., Jones, B.M., Jorgenson, M.T., Kent, K., 2020. Transferability of the deep learning mask R-CNN model for automated mapping of ice-wedge polygons in high-resolution satellite and UAV images. Remote Sens. 12, 1085. https://doi.org/10.3390/rs12071085.